# Negligible Magnetism in Excellent Structural Quality $Cr_xTi_{1-x}O_2$ Anatase: Contrast with High-$T_C$ Ferromagnetism in Structurally Defective $Cr_xTi_{1-x}O_2$

T. C. Kaspar,[1] S. M. Heald,[1] C. M. Wang,[1] J. D. Bryan,[2] T. Droubay,[1] V. Shutthanandan,[1] S. Thevuthasan,[1] D. E. McCready,[1] A. J. Kellock,[3] D. R. Gamelin,[2] and S. A. Chambers[1,*]

[1]*Pacific Northwest National Laboratory, Richland, Washington 99352, USA*
[2]*Department of Chemistry, University of Washington, Seattle, Washington 98195, USA*
[3]*IBM Almaden Research Center, San Jose, California 95120, USA*

(Received 1 July 2005; published 14 November 2005)

We reexamine the mechanism of ferromagnetism in doped $TiO_2$ anatase, using epitaxial Cr:$TiO_2$ with excellent structural quality as a model system. In contrast to highly oriented but defective Cr:$TiO_2$ ($\sim 0.5\mu_B$/Cr), these structurally superior single crystal films exhibit negligible ferromagnetism. Similar results were obtained for Co:$TiO_2$. We show for the first time that charge-compensating oxygen vacancies alone, as predicted by $F$-center mediated exchange, are not sufficient to activate ferromagnetism. Instead, the onset of ferromagnetism correlates with the presence of structural defects.

DOI: 10.1103/PhysRevLett.95.217203 PACS numbers: 75.25.+z, 75.50.Pp

Ferromagnetism (FM) at and above room temperature, and the associated spin polarization in the majority carrier band, are essential requirements for useful diluted magnetic semiconductors (DMSs) in spintronics. Since the first observation of room-temperature FM in Co-doped $TiO_2$ anatase [1], a number of reports of doped oxide film growth and magnetic properties have appeared in the literature that argue for the discovery of new high Curie temperature ($T_C$) oxide DMSs. With some exceptions [2–4], the magnetic moment per dopant has been found to be considerably less than expected from the number of unpaired $d$ electrons [5]. Additionally, FM has been measured in highly resistive specimens, showing that high concentrations of free carriers are not required to mediate the FM interaction. These observations have led to the suggestion that bound magnetic polaron (BMP) [6], or, for oxides, $F$-center- (FC) mediated [4] exchange interaction can result in FM. In this model, an FC BMP should be created when the incorporation of an aliovalent magnetic dopant into insulating, defect-free material requires the formation of an oxygen vacancy to maintain charge neutrality [3].

The structural quality of magnetically doped oxide films grown in investigations to date is considerably lower than that which typically characterizes heteroepitaxy of electronic materials. Missing from the field is a demonstration of very high quality epitaxial growth and a determination of magnetic properties in the absence of structural imperfections. In this Letter, we describe magnetic measurements for Cr-doped $TiO_2$ anatase with the highest degree of crystallographic perfection reported for any magnetically doped anatase to date. Chromium is of interest as a dopant because Cr-doped GaN and AlN exhibit high-temperature ferromagnetism [7,8], and because Cr is antiferromagnetic as a metal, precluding a spurious FM signal if metal segregation occurs. Earlier work by our group on Cr:$TiO_2$ revealed that highly oriented but rough films could be routinely grown by oxygen plasma assisted molecular beam epitaxy (OPAMBE) [9,10]. Cr(III) was found to substitute for Ti(IV), and was uniformly distributed. Additionally, such films were FM at and above room temperature ($T_C = 690$ K at $x = 0.1$), exhibiting an average saturation moment ($M_s$) of $\sim 0.5\mu_B$/Cr for $0.02 \leq x \leq 0.18$ in $Cr_xTi_{1-x}O_2$. This is significantly less than the expected value of $\sim 3\mu_B$/Cr for high-spin Cr(III), which is a $d^3$ system. Here we report on OPAMBE-grown material of much higher structural quality than previously published. Quite contrary to expectation, these films exhibit negligible ferromagnetism.

The key variables in determining the structural quality of $Cr_xTi_{1-x}O_2$ grown on $LaAlO_3$(001) and $SrTiO_3$(001) by OPAMBE are growth rate and substrate temperature. By reducing the growth rate from $\sim 0.1$ Å/sec at a substrate temperature of $\sim 700\,^\circ$C (hereafter referred to as "fast-grown") to $\sim 0.015$ Å/sec at a substrate temperature of $\sim 550\,^\circ$C (hereafter referred to as "slow-grown") without reducing the flux from the oxygen plasma source, layer-by-layer growth can be sustained, as judged by the persistence of reflection high energy electron diffraction (RHEED) intensity oscillations. Moreover, the structural quality and surface morphology are vastly improved at the lower growth rate.

We show in Fig. 1 typical transmission electron microscopy (TEM) high-resolution cross-sectional lattice images of slow- and fast-grown films, along with energy dispersive x-ray (EDX) spectra taken at two representative regions in each film—near the surface and near the substrate interface. The portion of the slow-grown film surface visible in the image is exceedingly flat, in contrast to the fast-grown material. These morphological differences are corroborated by RHEED (see insets to Fig. 2), x-ray reflectivity, and atomic force microscopy. The Cr is uniformly distributed for both growth rates, as seen in the representative

 

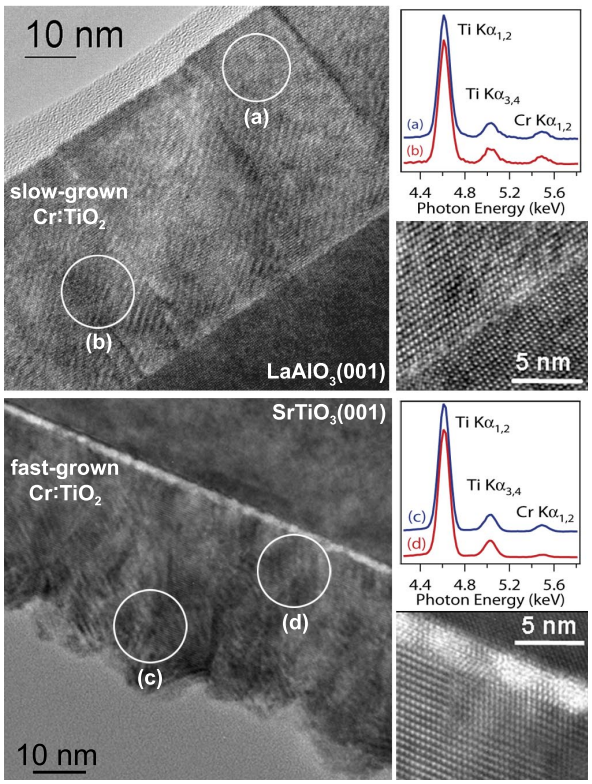


FIG. 1 (color online). TEM images and EDX spectra for Cr-doped $TiO_2$ grown at ~0.015 Å/sec and 550 °C (top), and ~0.1 Å/sec and 700 °C (bottom).

EDX spectra. The Ti-to-Cr ratios extracted from the EDX spectra are the same in the two regions of the slow-grown film (93 ± 1:7 ± 1%), revealing highly uniform Cr distribution. The ratios are 95 ± 1:5 ± 1% near the surface and 98 ± 1:2 ± 1% near the interface for the fast-grown film. The apparent Ti enrichment near the interface is due to a ~7 nm thick pure $TiO_2$ buffer layer deposited before introduction of the Cr dopant.

The volume-averaged differences in crystallographic quality are evident from high-resolution x-ray diffraction (XRD), as seen in Fig. 2. Here we show anatase (004) rocking curve measurements, along with a Gaussian fit to determine the peak width for the slow growth rate. The full width at half maximum is 0.095° for the slow-grown film [Fig. 2(a)], which after Scherrer analysis to quantify the broadening due to film thickness yields a mosaic spread of only 0.03°. The well-defined satellite fringes also indicate a very high degree of crystalline order. The asymmetry seen for the fast-grown film [Fig. 2(b)] is due to overlapping peaks from the distribution of crystallite orientations. Finally, slow-grown films show much lower Rutherford backscattering spectrometry channeling minimum yields. Typical numbers are ~7% (~8%) for Ti (Cr), compared to >40% (>40%) for Ti (Cr) for fast-grown films. Taken together, these data show that true single crystal epitaxy can only be achieved by growing at the slower rate.

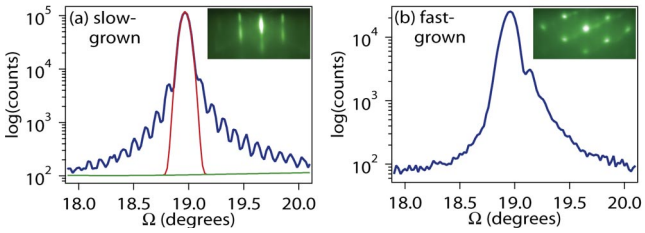


FIG. 2 (color online). Anatase (004) XRD rocking curves for $Cr:TiO_2/LaAlO_3(001)$, along with the [110] azimuth RHEED patterns obtained after deposition. (a) 450 Å of slow-grown $Cr_{0.07}Ti_{0.93}O_2$. (b) 560 Å of fast-grown $Cr_{0.10}Ti_{0.90}O_2$.

That Cr is primarily in a +3 charge state and substitutes for Ti is evident from Cr *K*-shell x-ray absorption near edge spectroscopy (XANES) and extended x-ray absorption fine structure (EXAFS), as seen in Fig. 3 for both fast-grown and slow-grown material. The inflection point along the leading edge for both $Cr:TiO_2$ films matches well that of $\alpha$-$Cr_2O_3$, whereas that of $CrO_2$ exhibits a chemical shift of ~2.5 eV to higher photon energy. Therefore, Cr in $Cr:TiO_2$ is predominantly in the +3 charge state. EXAFS for a slow-grown film deposited on $SrTiO_3$ [Fig. 3(b)] is well fit by calculations utilizing the FEFF computer program [11] in which Cr substitutes for Ti in the lattice. We also modeled various combinations of substitutional and interstitial site occupancies, and the fits (not shown) were much worse. The EXAFS for a fast-grown film deposited on $LaAlO_3$ is also shown in Fig. 3(b). Because of interference from the La *L*-edge absorption peak, the data cannot be reliably fit. However, there is good overlap between the EXAFS up to ~8 $Å^{-1}$ at the two growth rates, revealing Cr substitution for Ti at the higher growth rate as well.

In an effort to eliminate spurious magnetic signals, the as-received $LaAlO_3$ and $SrTiO_3$ substrates were etched in concentrated $HNO_3$ (back and sides only) to remove residual magnetic contamination resulting from dicing and

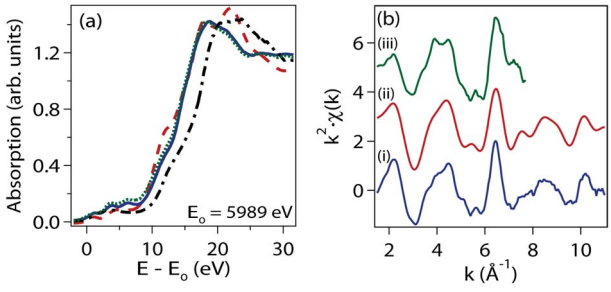


FIG. 3 (color online). (a) Cr *K*-shell XANES for 450 Å slow-grown $Cr_{0.08}Ti_{0.92}O_2/SrTiO_3(001)$ (solid line) and 400 Å fast-grown $Cr_{0.13}Ti_{0.87}O_2/LaAlO_3(001)$ (dotted line), along with epitaxial films of $\alpha$-$Cr_2O_3$ (dashed line) and $CrO_2$ (dot-dash line). (b) (i) Cr *K*-shell EXAFS for the slow-grown film, along with (ii) a model calculation for Ti lattice site occupancy; (iii) EXAFS for the fast-grown film.

handling; the absence of a detectable ferromagnetic signal was confirmed by room-temperature vibrating sample magnetometry (VSM) before growth. In fast-grown material, $M_s$ was found to be $\sim(0.2–0.8)\mu_B/\mathrm{Cr}$ with an average of $\sim(0.5–0.6)\mu_B/\mathrm{Cr}$ over many films, regardless of dopant concentration or film thickness. Contrary to the expectation that the structurally superior slow-grown material would exhibit $M_s$ values closer to the theoretical value of $\sim 3\mu_B/\mathrm{Cr}$, the $M_s$ values were found to be significantly *less* than those for fast-grown material, with most values in the range of $(0.05–0.15)\mu_B/\mathrm{Cr}$. For a typical film thickness of 450 Å, these values correspond to total measured moments of less than 10 $\mu$emu, as illustrated in Fig. 4(a). The stark contrast between hysteresis loops for slow- and fast-grown films is shown in Fig. 4(b). The $M_s$ values for slow-grown material are near the sensitivity limit of our VSM, and thus cannot be attributed with any confidence to intrinsic FM in slow-grown Cr:$TiO_2$ films. As an example, the measured $M_s$ of an *undoped* slow-grown anatase film is plotted in Fig. 4(a) and is comparable to those of doped slow-grown films. This result implies the measured signal may originate from magnetic contamination, presumably introduced or activated during deposition. However, it is clear from Fig. 4 that slow-grown material does not exhibit the strong magnetization observed in fast-grown films.

Samples are highly resistive ($\rho > \sim 5$ k$\Omega$ cm) as grown, as measured by four-point probe conductivity. The introduction of $n$-type carriers by vacuum reduction ($\rho \sim$ 1.0–0.1 $\Omega$ cm) provides a modest increase in $M_s$ (20–30%) for both fast- and slow-grown Cr:$TiO_2$, but does not account for the striking contrast in $M_s$ at the two growth rates. Low-temperature superconducting quantum interference device measurements confirm the low moments as well as the absence of ferromagnetic ordering between room temperature and 5 K. Substantial paramagnetism is observed below 50 K but cannot be quantified due to paramagnetic impurities in the substrates.

Although the role of electronic point defects has been discussed in detail for III-V DMSs [12], it has been implicitly assumed in all the primary models of ferromagnetism in DMSs and other ferromagnetic semiconductors that extended structural defects such as misfit dislocations and low-angle grain boundaries will detrimentally affect the ferromagnetic exchange. In superexchange and double exchange models, structural discontinuities in the lattice may disrupt the ionic "chains" participating in charge transfer. In both free carrier and FC BMP models, structural defects may create deep electronic states that trap carriers, interrupting or preventing ferromagnetic exchange. Thus, all these exchange models would predict the strongest ferromagnetic ordering in crystal lattices free of extended crystalline defects. However, it is clear from the results presented above that slow-grown Cr:$TiO_2$, which has a nearly perfect crystal structure, exhibits negligible ferromagnetic ordering. This is in contrast to faster-grown material, which exhibits both strong ferromagnetic ordering and a significant structural defect density. This finding brings into question the applicability of any of these exchange mechanisms, including the commonly cited FC BMP mechanism involving charge-compensating oxygen vacancies, to fully explain the ferromagnetic ordering in Cr:$TiO_2$.

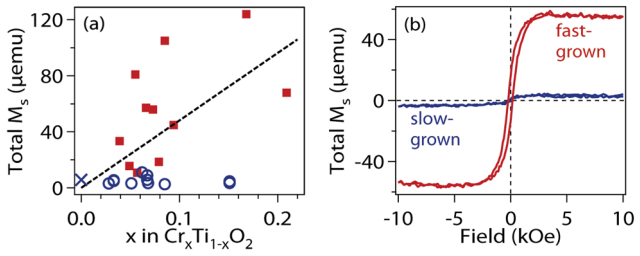


FIG. 4 (color online). (a) Total room-temperature $M_s$ vs Cr content for 450 Å slow-grown (open circles) and fast-grown (closed squares) $Cr_xTi_{1-x}O_2$. Cross is slow-grown undoped $TiO_2$. Dashed line is the expected dependence based on $0.5\mu_B/\mathrm{Cr}$. (b) Typical room-temperature VSM hysteresis loops for $\sim$450 Å $Cr_{0.07}Ti_{0.93}O_2$ at the two growth rates.

The absence of FM in structurally excellent slow-grown Cr:$TiO_2$ may be explained by all-electron full potential linearized augmented plane wave (FLAPW) density functional calculations for Cr:$TiO_2$ anatase by Ye *et al.* [13]. These calculations predict that FM will occur when uncompensated Cr(IV) dopants are present; such species are predicted to be strongly hybridized and form a FM ground state. In contrast, compensated Cr(III) ions are not predicted to interact, and in this case the ground state is predicted to be paramagnetic instead of ferromagnetic. As indicated in Fig. 3, the Cr dopant in both fast- and slow-grown material is predominantly Cr(III). The suppression of ferromagnetic exchange in slow-grown Cr:$TiO_2$ can thus be attributed to the lack of hybridization of the Cr(III) dopants. However, the ferromagnetic ordering in fast-grown Cr:$TiO_2$ cannot be explained by hybridization of Cr(IV), since this material contains little or no Cr(IV).

Cr-doped $TiO_2$ departs from true DMS character in important ways. Ferromagnetism is activated in this material by structural defects of a type that drastically degrades spin polarization in transport from (Mn, Zn)Se into GaAs/(Al, Ga)As [14]. When reduced, fast-grown Cr:$TiO_2$ exhibits neither an anomalous Hall effect nor x-ray magnetic circular dichroism at the Cr $L$ edge [15], in contrast to the prototypical DMS, Mn-doped GaAs. [16] Thus, the material is not expected to exhibit spin polarization in its reduced, semiconducting state, and is fundamentally different from Zener-type ferromagnetic DMSs such as Mn-doped GaAs.

A central conclusion of the present study is that the magnetic properties of Cr-doped $TiO_2$ anatase depend sensitively upon defects other than those introduced to

maintain charge neutrality as originally proposed in the FC BMP model [4,6]. Importantly, this conclusion appears to apply generally to doped $TiO_2$. Preliminary results for Co-doped $TiO_2$ [15] show that anatase films with high structural quality and uniform Co distribution can be obtained under slow growth conditions, and an analogous suppression of ferromagnetism is observed (fast: $\sim 1.2\mu_B$/Co [5], slow: $< \sim 0.1\mu_B$/Co). We propose that a similar sensitive dependence on structural defects is responsible for the wide diversity of observed magnetic results among magnetically doped oxides as a class. For example, grain boundary defects have been implicated in the activation of ferromagnetism by room-temperature aggregation of paramagnetic doped ZnO [17] and $TiO_2$ [18] nanocrystals under ambient conditions. The correlation between high-$T_C$ ferromagnetism and structural imperfections observed here for Cr-doped $TiO_2$, in the absence of any changes in Cr speciation or charge compensation, emphasizes the critical role extrinsic lattice defects play in governing the magnetism of this class of materials.

Although differing in its details, the strong dependence of FM on structural lattice defects may remain generally consistent with a BMP description of FM in Cr-doped $TiO_2$. While we have shown that charge-compensating oxygen vacancies occurring in an otherwise perfect crystal lattice are not sufficient to induce strong ferromagnetic ordering, we speculate that extended structural defects give rise to charged point defects of a fundamentally different type. The precise identities of the activating defects are not yet clear, but it is reasonable to associate them with oxygen vacancies [19]. Within the BMP model [4,6], bound carriers associated with these defects occupy a volume $\gamma^3$ and are responsible for coupling remote $Cr^{3+}$ ions within this volume. The greater density ($\delta$) of structural imperfections in the fast-grown films yields a greater overall volume occupied by BMPs ($\delta\gamma^3$), thus increasing their probability of coalescence into ferromagnetic domains. Experiments to address the microscopic identities of the activating defects are currently underway.

The authors are grateful to L. Ye and A. J. Freeman for making available their FLAPW calculations prior to publication, and to J. E. Jaffe for helpful discussions. This work was performed in the Environmental Molecular Sciences Laboratory, a national scientific user facility sponsored by the Department of Energy's Office of Biological and Environmental Research and located at Pacific Northwest National Laboratory. This work was supported by the US Department of Energy, Office of Science, Office of Basic Energy Sciences, Division of Materials Science and Engineering Physics. Work at UW was funded by the NSF (DMR-0239325 and ECS-0224138) and the Research Corporation. T. C. K. acknowledges support from the PNNL/University of Washington Joint Institute for Nanoscience. Use of the Advanced Photon Source was supported by the U.S. Department of Energy, Office of Science, Office of Basic Energy Sciences.

*Electronic address: sa.chambers@pnl.gov

[1] Y. Matsumoto *et al.*, Science **291**, 854 (2001).
[2] S. B. Ogale *et al.*, Phys. Rev. Lett. **91**, 077205 (2003).
[3] J. M. D. Coey *et al.*, Appl. Phys. Lett. **84**, 1332 (2004).
[4] J. M. D. Coey, M. Venkatesan, and C. B. Fitzgerald, Nat. Mater. **4**, 173 (2005).
[5] S. A. Chambers and R. F. Farrow, MRS Bull. **28**, 729 (2003).
[6] A. Kaminski and S. Das Sarma, Phys. Rev. Lett. **88**, 247202 (2002).
[7] H. X. Liu *et al.*, Appl. Phys. Lett. **85**, 4076 (2004).
[8] R. M. Frazier *et al.*, Appl. Phys. Lett. **86**, 052101 (2005).
[9] T. Droubay *et al.*, J. Appl. Phys. **97**, 046103 (2005).
[10] J. Osterwalder *et al.*, Thin Solid Films **484**, 289 (2005).
[11] S. I. Zabinsky *et al.*, Phys. Rev. B **52**, 2995 (1995).
[12] C. Timm, J. Phys. Condens. Matter **15**, R1865 (2003).
[13] L. Ye and A. J. Freeman (unpublished).
[14] R. M. Stroud *et al.*, Phys. Rev. Lett. **89**, 166602 (2002).
[15] T. C. Kaspar *et al.* (unpublished).
[16] Y. L. Soo *et al.*, Phys. Rev. B **67**, 214401 (2003).
[17] P. V. Radovanovic and D. R. Gamelin, Phys. Rev. Lett. **91**, 157202 (2003).
[18] J. D. Bryan *et al.*, J. Am. Chem. Soc. **126**, 11 640 (2004).
[19] J. D. Bryan *et al.*, J. Am. Chem. Soc. **127**, 15 568 (2005).